

Nuclear Responses to Two-Body External Fields Studied with the Second Random-Phase-Approximation

Futoshi Minato^{1, 2, *}

¹Department of Physics, Kyushu University, Fukuoka 819-0395, Japan

²RIKEN Nishina Center for Accelerator-Based Science, Wako, Saitama 351-0198, Japan

(Dated: December 24, 2025)

This study investigates nuclear responses to two-body external fields, interpreted as double-phonon excitations, within the subtracted second random-phase approximation (SSRPA) for ^{16}O . To clarify the underlying characteristics of these modes, Hartree-Fock (HF) and SSRPA with the diagonal approximation are first examined. The resulting strength distributions are nearly identical, indicating that residual interactions in the $1p-1h$ sector contribute only weakly. This behavior contrasts with that of one-body excitations, where coupling between $1p-1h$ and $2p-2h$ configurations is essential for generating collectivity. In the full SSRPA calculation, which incorporates the residual interaction among $2p-2h$ configurations, the strength distributions are substantially modified. The double IS 0^+ and 2^+ modes show pronounced redistribution, with peaks shifted to lower energies and additional strength emerging at higher energies, whereas the double IV 1^- mode shifts predominantly to higher energies due to a largely repulsive interaction. Analysis of single transition amplitudes reveals that low-lying resonances are formed coherently through constructive neutron-neutron, proton-proton, and neutron-proton configurations, while high-lying resonances are dominated by neutron-proton configurations, reflecting their higher state density. These results demonstrate that double-phonon excitations cannot be described by simple folding of one-body responses; a fully microscopic treatment of $2p-2h$ mixing, as provided by SSRPA, is essential.

I. INTRODUCTION

Collective motions are general properties of many-body systems and can be found in electronic systems, biological systems, human society, and so on. The nucleus is also one of the many-body systems in nature. Its characteristic feature is that it consists of two types of barions, protons and neutrons, and its dynamics are governed by quantum mechanics with spin and isospin degrees of freedom. In addition, the nucleus is considered to be an isolated system, allowing one to study quantum many-body problems without external interference. As a result, nuclei have exhibited many intriguing collective motions and have provided important insights into the behavior of quantum many-body systems.

A typical collective motion of the nucleus is surface vibration and rotation. In particular, surface vibrations have attracted considerable interests from researcher because of their similarity to collective motions in other many-body systems. In the first order, nuclear surface vibrations are generally interpreted as collective one-particle-one-hole ($1p-1h$) excitations. One of the most succeeded models in this context is the random-phase approximation (RPA) [1–3]. In particular, self-consistent RPA approaches built on top of the energy density functional (EDF), which have the advantage of avoiding additional phenomenological parameters besides those determined from the nuclear bulk properties, have achieved remarkable successes over the last two decades. RPA has also been extended to the description of nuclear reactions

in both continuum form [4–7] and discrete form [8, 9]. It has provided valuable insights into the mechanisms of nuclear excitation modes and has played a key role in advancing nuclear structure studies.

A model that goes beyond the RPA is the second random-phase approximation (SRPA) [10], which extends the description of nuclear excitations by including up to two-particle-two-hole ($2p-2h$) configurations. A major advantage of SRPA is that it can account for the spreading width (damping effect), thereby enabling a more direct comparison with experimental data. This approach has been studied and developed by several groups [11–13]. With the increase in computational resources, this approach has been extended to a self-consistent framework [14–16]. However, when applied with effective interactions, SRPA encounters the problem of double-counting of higher-order correlations. To address this issue, the subtracted SRPA (SSRPA) was proposed, introducing a subtraction method [17, 18]. This approach has proven successful in describing experimental strength distributions and has been widely applied to studies of the spreading widths of giant resonances [18, 19] and the quenching of Gamow-Teller transitions [20–24]. Here, we should also mention that another class of approaches beyond RPA is provided by particle-vibrational coupling [25, 26], relativistic quasi-particle time-blocking approximation [27], two-phonon models [28–32], and the small amplitude limit of the time-dependent density-matrix theory [33].

Models beyond RPA are frequently applied to the study of double-phonon excitations, that is, excitations in which one phonon is built on top of another [34, 35]. Such excitations are considered to be induced either by the sequential action of one-body external fields or

* E-mail: minato.futoshi.009@m.kyushu-u.ac.jp

by direct action of two-body external fields, and have been investigated both experimentally and theoretically in proton-capture reactions [36], heavy-ion reactions [37–39], and pion double-charge-exchange reactions [40, 41]. Theoretical approaches based on multiphonon models [28–32, 42, 43] and a semiclassical formalism [44] have also been developed independently. Some of them are also applied to calculate heavy-ion reactions [44, 45] (For further details, see also Refs. [34, 35, 38]). The SSRPA framework enables the study of nuclear excitations induced by both the sequential operation of one-body external fields and the direct action of two-body external fields [16, 33]. The former corresponds to a specific channel of sequential excitation (e.g. double quadrupole excitations coupled to a certain angular momentum), while the latter directly probes the doorway state of nuclear resonances. Although nuclear excitations due to one-body external fields have been extensively studied, those induced by two-body external fields remain poorly understood. A comprehensive microscopic understanding of nuclear excitations driven by two-body external fields is therefore essential.

Two-body external fields are also substantial importance for muon-nuclear capture and electromagnetic nuclear reactions through meson-exchange two-body currents (MEC). We recently investigated the effect of MEC on particle emissions following negative-muon capture in nuclei within the second Tamm-Dancoff approximation (STDA) [46]. As previously noted in Ref. [47], the importance of MEC in reproducing high-energy proton emissions was confirmed by incorporating a phenomenological MEC contribution into our theoretical framework. Although STDA, an extension of TDA to include $2p-2h$ configurations, is, in principle, capable of taking MEC effects into account, we did not pursue this because of complicated structure of the MEC operators. Our current project is to study nuclear responses to two-body external fields within the SSRPA framework, with the aim of extending it to microscopically incorporate MEC effects in muon capture as well as in other weak and electromagnetic processes in the future. In this paper, we discuss nuclear collective motions induced by non-charge-exchange two-body external fields. In particular, we focus on 0^+ components of double multipole excitations of ^{16}O .

The structure of this paper is as follows. In Sect. II we describe the theoretical framework used in this study. Sect. III presents and discusses the result, and Sect. IV provides a summary of the findings and conclusions.

II. THEORETICAL FRAMEWORK OF SSRPA

A. SSRPA formalism

Although the basic framework of SRPA has been introduced in many literature [10–13, 16, 18, 19, 48], here we demonstrate it briefly because some of quantities are

essential for discussing our results. Excited states with spin J and its projection on z -axis M are approximated by $|\nu; JM\rangle = Q_{\nu; JM}^\dagger |\text{SRPA}\rangle$ with $Q_{\nu; JM}^\dagger$ being the SRPA phonon creation operator defined as

$$Q_{\nu; JM}^\dagger = \sum_{ph} \left(X_{\nu; ph}^{(J)} O_{ph}^{(JM)\dagger} - (-1)^{J+M} Y_{\nu; ph}^{(J)} O_{ph}^{J-M} \right) \\ + \sum_{\substack{p_1 < p_2 \\ h_1 < h_2}} \left(\mathcal{X}_{\nu; p_1 p_2 h_1 h_2}^{(J_p J_h) J} O_{p_1 p_2 h_1 h_2}^{(J_p J_h) JM\dagger} \right. \\ \left. - (-1)^{J+M} \mathcal{Y}_{\nu; p_1 p_2 h_1 h_2}^{(J_p J_h) J} O_{p_1 p_2 h_1 h_2}^{(J_p J_h) J-M} \right). \quad (1)$$

and $|\text{SRPA}\rangle$ is the SRPA correlated ground state. We denote particle and hole states of single-particle states as p and h , respectively. The single-particle energies and wave functions are calculated within the Skyrme energy-density functionals under the spherical symmetry using the SGII force [49]. The continuum states are discretized by assuming a box size of 20 fm with a step of 0.1 fm. The operators $O_{ph}^{(JM)\dagger}$ and $O_{p_1 p_2 h_1 h_2}^{(J_p J_h) JM\dagger}$ create $1p-1h$ and $2p-2h$ states, respectively, and J_p and J_h are the spins formed by 2 particles and 2 holes, respectively. The detailed form can be found in Ref. [13, 16]. It is worth noting that one needs to avoid double counting in particle and hole configurations so that the sums in Eq. (1) run over $p_1 < p_2$ and $h_1 < h_2$. Neglecting the terms of $\mathcal{X}_{\nu; p_1 p_2 h_1 h_2}^{(J_p J_h) J}$ and $\mathcal{Y}_{\nu; p_1 p_2 h_1 h_2}^{(J_p J_h) J}$, the formalism corresponds to the standard $1p-1h$ RPA. The coefficients of $X_{\nu; ph}^{(J)}$, $Y_{\nu; ph}^{(J)}$, $\mathcal{X}_{\nu; p_1 p_2 h_1 h_2}^{(J_p J_h) J}$, $\mathcal{Y}_{\nu; p_1 p_2 h_1 h_2}^{(J_p J_h) J}$, and SRPA phonon energy are determined by solving the SRPA equation:

$$\begin{pmatrix} A & B \\ -B^* & -A^* \end{pmatrix} \begin{pmatrix} X_\nu^{(J)} \\ Y_\nu^{(J)} \end{pmatrix} = \hbar\omega \begin{pmatrix} X_\nu^{(J)} \\ Y_\nu^{(J)} \end{pmatrix} \quad (2)$$

with

$$A = \begin{pmatrix} A_{11'} & A_{12'} \\ A_{21'} & A_{22'} \end{pmatrix}, \quad B = \begin{pmatrix} B_{11'} & B_{12'} \\ B_{21'} & B_{22'} \end{pmatrix} \quad (3)$$

and

$$X_\nu^{(J)} = \begin{pmatrix} X_\nu^{(J)} \\ \mathcal{X}_\nu^{(J_p J_h) J} \end{pmatrix}, \quad Y_\nu^{(J)} = \begin{pmatrix} Y_\nu^{(J)} \\ \mathcal{Y}_\nu^{(J_p J_h) J} \end{pmatrix}. \quad (4)$$

The index numbers 1 and 2 denote $1p-1h$ (ph) and $2p-2h$ ($p_1 p_2 h_1 h_2$) configurations, respectively. The block matrix of $A_{11'}$, the matrix elements $A_{ph'hp'}$, represent the transition between $1p-1h$ states due to the particle-hole residual interaction and have the same form as the ordinary $1p-1h$ RPA [3]. So $B_{11'}$ does. On the other hand, $A_{12'}$, $A_{21'}$, $B_{12'}$, and $B_{21'}$ are the block matrix for the transition between $1p-1h$ and $2p-2h$ states. The matrix elements of $A_{22'}$ and $B_{22'}$ are the ones for the transition between $2p-2h$ states. In this work, the matrix elements for $A_{11'}$ and $B_{11'}$ are estimated by the second derivative of energy density with respect to density, while those for other block matrices are calculated directly from the Skyrme force, being $B_{12'} = B_{21'} = B_{22'} = 0$ [14].

It is known that strength distributions calculated by SRPA are significantly smaller than the $1p-1h$ RPA, because some of matrix elements of the two-body force are already taken into account in the Skyrme-HF [17]. To overcome this problem, the subtraction method is applied to SRPA [18], and denoted as SSRPA. We do not go into detail about SSRPA in this paper; however the validity has been discussed in some papers [18–20]. In the subtracted method, $A_{11'}$ block matrix of SSRPA is modified as

$$A_{11'}^{(S)} = A_{11'} + \sum_{22'} A_{12} A_{22'}^{-1} A_{2'1'}, \quad (5)$$

while the other block matrices remain the same.

If the coupling among the $2p-2h$ configurations is neglected, the $A_{22'}$ block will become diagonal. In this situation, it is given by

$$A_{22'}^{(D)} = \delta_{p_1 p'_1} \delta_{p_2 p'_2} \delta_{h_1 h'_1} \delta_{h_2 h'_2} E_{p_1 h_1 p_2 h_2}, \quad (6)$$

where the unperturbed $2p-2h$ energy is $E_{p_1 h_1 p_2 h_2} = \varepsilon_{p_1} + \varepsilon_{p_2} - \varepsilon_{h_1} - \varepsilon_{h_2}$. Here, ε_p and ε_h are the single-particle energies of particle and hole states, respectively, obtained from the Skyrme-HF calculation. This diagonal approximation is effective in reducing the computational cost because it allows us to avoid calculating the inverse matrix in Eq. (5). To examine the impact of the diagonal approximation within the SSRPA framework, we consider two cases: (1) SSRPA_F, the full SSRPA calculation without any diagonal approximation; (2) SSRPA_D, in which the diagonal approximation is applied both to the subtraction method in Eq. (5) and to $A_{22'}$ in Eq. (3). In the next section, we also compare these results with those obtained from the HF calculation, which neglects all residual interactions. Namely, $A_{11'} = (\varepsilon_p - \varepsilon_h) \delta_{pp'} \delta_{hh'}$, $A_{12'} = A_{21'} = 0$, $B_{11'} = 0$, and $A_{22'} = A_{22'}^{(D)}$.

The adopted model space is defined as follows. Single-particle levels with energies up to $\varepsilon_p < 100$ MeV are included. Non-perturbed $1p-1h$ excitation energies are taken into account up to 100 MeV, and $2p-2h$ configurations are included up to 100, 80 and 60 MeV for the 0^+ , 1^- , and 2^+ states of ^{16}O , respectively. Within this model space, the resulting strength distributions are sufficiently converged. In particular, a large model space is essential to achieve adequate convergence for the strength distributions of two-body excitations.

B. Strength distribution

Provided that J is the multipolarity of the external field and M its projection onto the z -axis, the strength distribution of a one-body external field without a spin operator is given by

$$|\langle \nu, J || F_J || \text{SRPA} \rangle|^2 \approx \left| \sum_{ph} C_{\nu;ph}^{(J)} \right|^2, \quad (7)$$

where F_{JM} may represent the isoscalar (IS) monopole ($r^2 Y_{00}$), isovector (IV) dipole ($r Y_{1M} \tau_z$), or IS quadrupole ($r^2 Y_{2M}$) operator. The strength distribution associated with a two-body external field, $\mathcal{F}_{JM;L_1 L_2} \equiv [F_{L_1} G_{L_2}]^{JM}$ (where G is another one-body external operator), is given by

$$|\langle \nu, J || \mathcal{F}_{J;L_1 L_2} || \text{SRPA} \rangle|^2 \approx \left| \sum_{p_1 < p_2} \sum_{J_p J_h} C_{\nu;p_1 p_2 h_1 h_2}^{(J_p J_h; L_1 L_2) J} \right|^2, \quad (8)$$

respectively. The single $1p-1h$ transition amplitude $C_{\nu;ph}^{(J)}$ and the single $2p-2h$ transition amplitude $C_{\nu;p_1 p_2 h_1 h_2}^{(J_p J_h; L_1 L_2) J}$ represent the contribution to resonance strength from $1p-1h$ and $2p-2h$ configurations, respectively, and defined as

$$C_{\nu;ph}^{(J)} = \left(X_{\nu;ph}^{(J)} + (-)^J Y_{\nu;ph}^{(J)} \right) F_{ph}^{(J)} \quad (9)$$

$$\begin{aligned} & C_{\nu;p_1 p_2 h_1 h_2}^{(J_p J_h; L_1 L_2) J} \\ &= \left(\mathcal{X}_{\nu;p_1 p_2 h_1 h_2}^{(J_p J_h) J} + (-)^{L_1 + L_2} \mathcal{Y}_{\nu;p_1 p_2 h_1 h_2}^{(J_p J_h) J} \right) \mathcal{F}_{p_1 p_2 h_1 h_2}^{(J_p J_h; L_1 L_2) J}. \end{aligned} \quad (10)$$

In the following discussion, we omit the superscripts and subscripts of C for brevity. The reduced transition strength $F_{ph}^{(J)}$ is

$$F_{ph}^{(J)} = \langle p || F_J || h \rangle \equiv \langle j_p l_p || F_J || j_h l_h \rangle, \quad (11)$$

and

$$\begin{aligned} \mathcal{F}_{p_1 p_2 h_1 h_2}^{(J_p J_h) J} &= 2 \sqrt{\frac{(2J_p + 1)(2J_h + 1)}{(1 + \delta_{p_1 p_2})(1 + \delta_{h_1 h_2})}} \left[\begin{pmatrix} j_{p_1} & j_{p_2} & J_p \\ j_{h_1} & j_{h_2} & J_h \\ L_1 & L_2 & J \end{pmatrix} \right. \\ &\quad \times F_{p_1 h_1}^{(L_1)} G_{p_2 h_2}^{(L_2)} - (-)^{j_{h_1} + j_{h_2} - J_h} \left. \begin{pmatrix} j_{p_1} & j_{p_2} & J_p \\ j_{h_2} & j_{h_1} & J_h \\ L_1 & L_2 & J \end{pmatrix} F_{p_1 h_2}^{(L_1)} G_{p_2 h_1}^{(L_2)} \right]. \end{aligned} \quad (12)$$

Analyzing the single transition amplitudes defined in Eqs. (9) and (10) provides insight into the collectivity of a given resonance state ν . A notable feature of two-body external fields is that their collectivity differs from that of one-body external fields, which excite only proton $1p-1h$, neutron $1p-1h$, or a mixture of the two. Since a $2p-2h$ configuration consists of two $1p-1h$ excitations, and each $1p-1h$ excitation may involve either proton or neutron transitions, the resulting $2p-2h$ configuration can be built from neutron-neutron (nn), proton-proton (pp), or neutron-proton (np) components. Here, nn and pp denote configurations in which both $1p-1h$ excitations involve neutrons or protons, respectively, while np denotes configurations in which one excitation involves neutrons and the other involves protons.

In this work, we investigate the $J^\pi = 0^+$ components of two-body external fields, i.e., double multipole excitations defined as

$$\mathcal{F}_{0;00} = \left[[r^2 Y_0][r^2 Y_0] \right]^0 \quad (13)$$

$$\mathcal{F}_{0;11} = \left[[r^1 Y_1 \tau_z][r^1 Y_1 \tau_z] \right]^0 \quad (14)$$

$$\mathcal{F}_{0;22} = \left[[r^2 Y_2][r^2 Y_2] \right]^0. \quad (15)$$

These modes may be interpreted either as sequential actions of the corresponding one-body external fields or as direct actions of the two-body external fields. For convenience, we refer to the external fields defined in Eqs. (13), (14), and (15) as the double IS monopole (0^+), double IV dipole (1^-), and double IS quadrupole (2^+) modes, respectively.

The strength distribution folded by a Lorentzian function of width Γ_0 is defined as

$$L_J(E) = \sum_{\nu} |\langle \nu, J | \mathcal{O}_J | \text{SRPA} \rangle|^2 \frac{1}{\pi} \frac{\Gamma_0/2}{(E - E_{\nu})^2 + (\Gamma_0/2)^2}, \quad (16)$$

where \mathcal{O}_J takes F_J and $\mathcal{F}_{J;L_1 L_2}$. The centroid energy is defined as m_1/m_0 , where m_k is the k -th order energy weighted sum-rule

$$m_k = \sum_{\nu} (\hbar\omega_{\nu})^k |\langle \nu, J | \mathcal{O}_J | \text{SRPA} \rangle|^2. \quad (17)$$

III. RESULT

In this section, we present the strength distributions for both one-body and two-body external fields. Since these two types of excitations are closely related, discussing them together provides a more coherent physical picture of the strength distributions induced by two-body external fields.

A. Strength distributions of one-body external fields

First, we discuss the ordinary IS monopole (0^+), IV dipole (1^-), and IS quadrupole (2^+) excitations before turning to the double multipole excitations. These modes have already been analyzed in Refs. [15, 16, 18, 19, 50], but they are again presented here for reference and for use in later discussions.

Figure 1 shows the IS monopole excitation strength distribution of ^{16}O , calculated using RPA, SSRPA_F, and SSRPA_D with the SGII interaction [49]. The calculated strength distributions are folded with a Lorentzian function of width $\Gamma_0 = 1$ MeV. Both RPA and SSRPA (SSRPA_F and SSRPA_D) exhibit IS 0^+ strength distributed over the excitation energy range

of $\hbar\omega = 10\text{--}40$ MeV. The dominant $1p\text{--}1h$ configurations contributing the resonances in this energy range are $[np_{1/2}][0p_{1/2}]^{-1}$ and $[np_{3/2}][0p_{3/2}]^{-1}$ ($n = 2, 3, 4$) for both neutron and proton.

The damping effect, which arises from coupling to $2p\text{--}2h$ configurations, appears to be weak in SSRPA_F and SSRPA_D. This weak damping is understood as a cancellation between incoherent and coherent contributions to the self-energy for non-spin-flip isoscalar monopole excitations, as discussed in Ref. [11]. Although SSRPA_F and SSRPA_D exhibit noticeable differences, indicating that coupling among $2p\text{--}2h$ configurations has a non-negligible impact on the strength distributions, the overall structure is already captured reasonably well by SSRPA_D. Figure 2 shows the corresponding results for the IV 1^- excitation. The dominant $1p\text{--}1h$ configurations contributing the resonances in the $\hbar\omega = 10\text{--}30$ MeV region are $[nd_{5/2}][0p_{3/2}]^{-1}$, $[nd_{3/2}][0p_{1/2}]^{-1}$ ($n = 0, 1, 2$), and $[ns_{1/2}][0p_{3/2}]^{-1}$ and $[ns_{1/2}][0p_{1/2}]^{-1}$ ($n = 1, 2$) for both neutron and proton. Figure 3 displays the results for the IS 2^+ mode. The qualitative behavior of RPA and SSRPA is similar to that seen in the IS 0^+ case; however, in contrast to the monopole excitation, the IS 2^+ mode exhibits a pronounced damping effect.

We also estimated the center energies (E_c) and widths (Γ_c) of the strength distributions for the three types of excitations. These quantities were obtained by fitting L_J in Eq. (16) with another Lorentzian function,

$$L_{\text{fit}}(E) = N \times \frac{1}{\pi} \frac{2}{\Gamma} \frac{1}{(E - E_c)^2 + (\Gamma_c/2)^2}, \quad (18)$$

where the normalization factor N is determined simultaneously with E_c and Γ_c through a least-squares fitting procedure. The physical width is then obtained following Ref. [51] as

$$\Gamma \approx \Gamma_c - \Gamma_0. \quad (19)$$

Table I lists the center energies and widths extracted from the Lorentzian fits, and centroid energies of the IS 0^+ , IV 1^- , and IS 2^+ resonances calculated using RPA and SSRPA_F. To distinguish these quantities from those corresponding to the strength distributions of the two-body external fields discussed in the next section, we use superscripts "“(1)”, namely $E_c^{(1)}$ and $\Gamma^{(1)}$. The center energies obtained with SSRPA_F are shifted to lower values by about 3.4, 2.8, and 1.6 MeV for the IS 0^+ , IV 1^- , and IS 2^+ modes, respectively. This shift can be understood as follows. Coupling to $2p\text{--}2h$ configurations redistributes part of the strength to higher excitation energies, which in turn pushes the dominant resonance to lower energies so as to satisfy the relevant sum-rule constraint. Although SSRPA_F does not strictly fulfill the energy-weighted sum-rule, the same reasoning applies to the inverse energy-weighted sum-rule which SSRPA_F fulfills [18, 19]. The widths obtained with SSRPA_F are smaller than those from RPA for the IS 0^+ mode, whereas the width for the IV 1^- mode remains essentially unchanged. However, non-negligible strength distributions

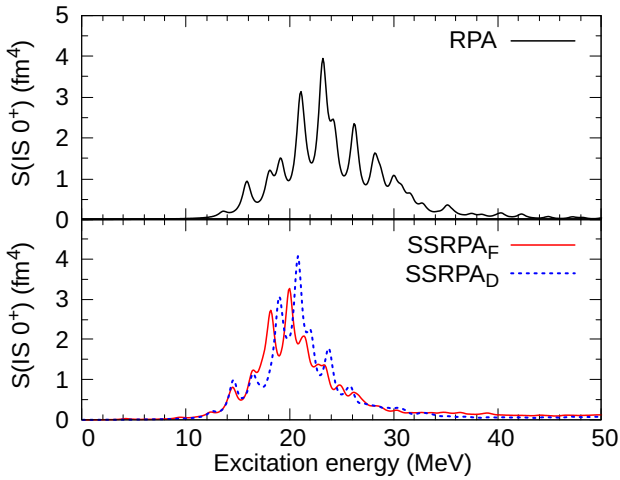


FIG. 1. Strength distribution of IS 0^+ excitations in ^{16}O calculated by RPA (top) and three types of SSRPA (bottom). The distributions are folded with a Lorentzian function of width $\Gamma_0 = 1$ MeV.

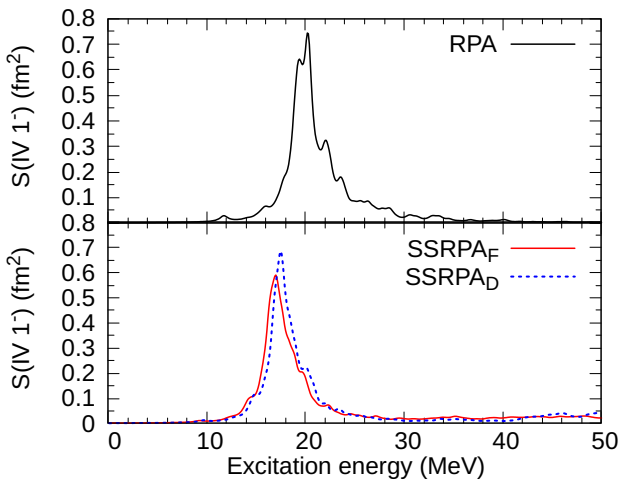


FIG. 2. Same as Fig. 1, but for IV 1^- excitations.

exist beyond the main peak positions, which cannot be fully captured by the Lorentzian fitting adopted in Eq. (18). Therefore, the smaller widths do not necessarily indicate a weaker effect of $2p$ - $2h$ configuration mixing. Therefore, the centroid energies m_1/m_0 obtained with SSRPA_F are systematically larger than those of RPA. In contrast, the width obtained with SSRPA_F is significantly larger than that from RPA for the IS 2^+ mode, where the $2p$ - $2h$ configuration mixing directly affects the main peak structure. These results will be compared with the center energies, widths, and centroid energies of the strength distributions for the two-body external fields in the next section.

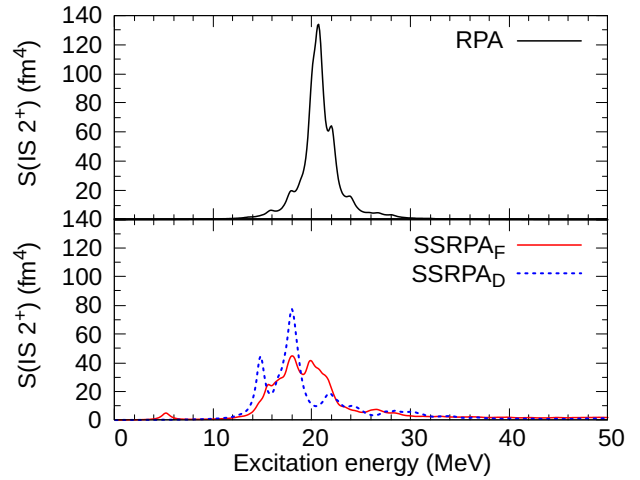


FIG. 3. Same as Fig. 1, but for IS 2^+ excitations.

TABLE I. Center energies $E_c^{(1)}$ and widths $\Gamma^{(1)}$ extracted from the Lorentzian fits, and the centroid energy m_1/m_0 of the strength distributions of the IS 0^+ , IV 1^- , and IS 2^+ obtained from RPA and SSRPA_F.

Mode	$E_c^{(1)}$ (MeV)		$\Gamma^{(1)}$ (MeV)		m_1/m_0 (MeV)	
	RPA	SSRPA _F	RPA	SSRPA _F	RPA	SSRPA _F
IS 0^+	23.3	19.9	6.9	5.2	24.8	30.9
IV 1^-	20.0	17.2	2.0	2.0	21.9	27.6
IS 2^+	20.6	19.0	1.1	4.8	20.9	25.3

B. Strength distributions of two-body external fields

The strength distributions of the two-body external fields constitute one of the main focuses of this work. However, the basic properties of these strength distributions are not necessarily well understood. Therefore, we first present the results obtained with the HF method, which provide the essential physical picture of the nuclear responses to double-multipole excitations. We then discuss the characteristics of the strength distributions calculated with SSRPA_F.

1. HF calculation

Figure 4 shows the strength distributions for the IS 0^+ , IV 1^- , and IS 2^+ modes obtained from HF (the upper panels), and the 0^+ components of the two-body external fields defined in Eqs. (13)-(15) for ^{16}O obtained from HF and SSRPA_D calculations (the lower panels). Since the HF results represent non-collective excitations, one may be concerned about their dependence on the model space, particularly on the box size (i.e., the treatment of continuum states). We have verified that, although the detailed fine structures of the strength distributions are sensitive to the model space, the overall locations of the

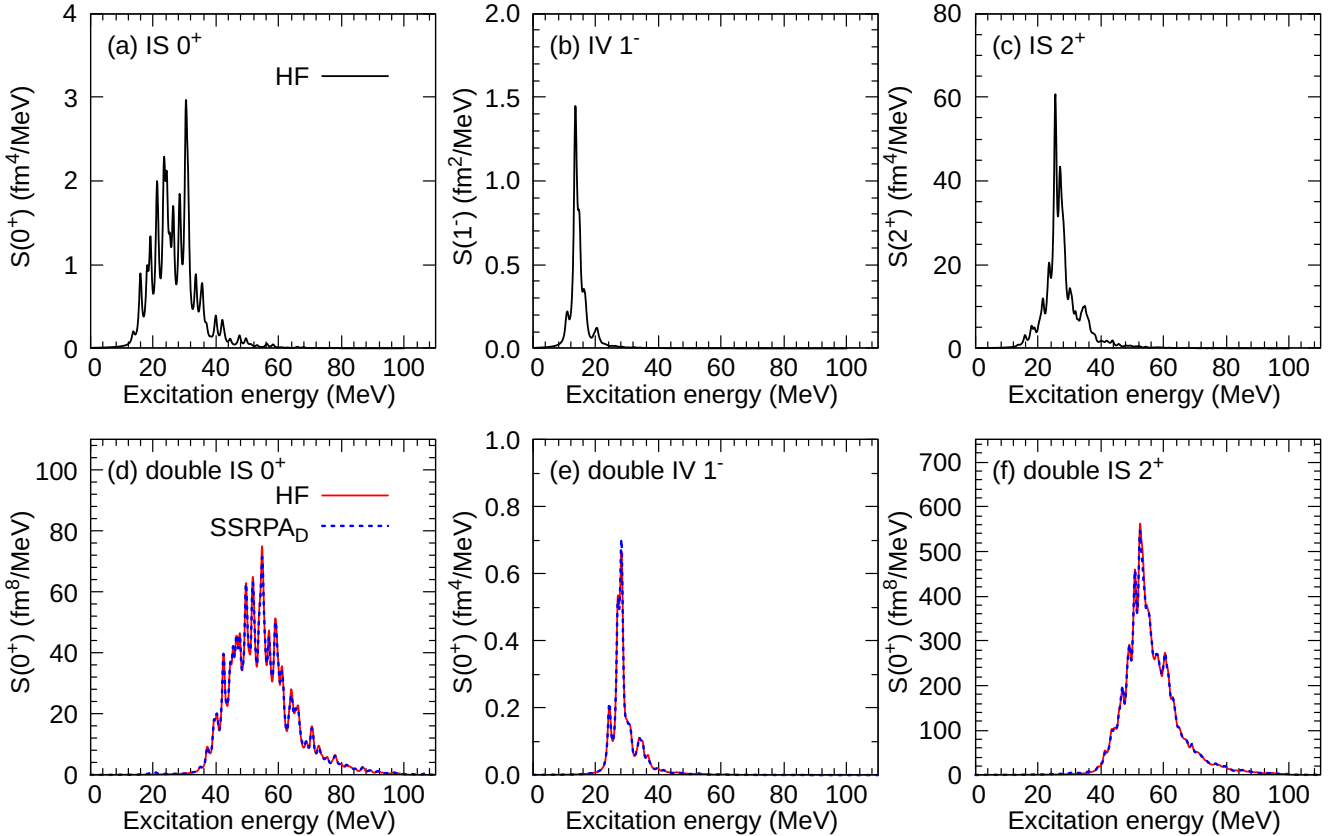


FIG. 4. (a)–(c) Strength distributions of the one-body external fields for the IS 0^+ , IV 1^- , and IS 2^+ modes obtained with HF. (d)–(f) Strength distributions of the corresponding double multipole modes, defined in Eqs. (13)–(15), obtained with HF and SSRPA_D.

main structure remain essentially unchanged.

Intuitively, the strength distributions of the two-body external fields obtained from the HF calculation are expected to appear at approximately twice the excitation energies of the corresponding one-body external fields. This tendency is indeed observed when comparing the strength distributions of the one-body and two-body external fields shown in Fig. 4. To quantify this observation, the center energies and widths estimated from Eq. (18) are summarized in Table II. The center energies of the two-body external fields are found to be close to twice those of the corresponding one-body external fields, consistent with the intuitive expectation. In contrast, the widths do not exhibit a universal behavior: while the width for the double IS 2^+ mode increases by more than a factor of two, those for the IS 0^+ and the IV 1^- modes show only moderate increases.

We also find that the results of SSRPA_D nearly overlap with those of HF. According to Eq. (2), the difference between SSRPA_D and HF originates from the residual interaction in $A_{11'}$ and $A_{12'}$ ($A_{21'}$), both of which are absent in the HF calculation. This indicates that the contributions of these matrix elements are rather limited for the strength distributions induced by two-body external fields. This behavior contrasts with the case of one-body

TABLE II. Center energies and widths of the IS 0^+ , IV 1^- , and IS 2^+ modes ($E_c^{(1)}$ and $\Gamma^{(1)}$), and of the 0^+ component of the corresponding double multipole modes obtained from HF calculations ($E_c^{(2)}$ and $\Gamma^{(2)}$). All values are given in MeV.

Mode	one-body		two-body		
	$E_c^{(1)}$	$\Gamma^{(1)}$	Mode	$E_c^{(2)}$	$\Gamma^{(2)}$
IS 0^+	26.0	12.1	double IS 0^+	52.8	15.4
IV 1^-	13.8	1.2	double IV 1^-	27.8	1.8
IS 2^+	26.3	3.9	double IS 2^+	53.5	9.9

external fields, where the coupling between $1p-1h$ and $2p-2h$ configurations plays a significant role, as seen in Figs. 1–3. The present results suggests that transitions from $1p-1h$ to the $2p-2h$ configurations dominate over the reverse process, effectively leading to an effective decoupling between the two spaces. In this sense, treating the $1p-1h$ and $2p-2h$ blocks as decoupled in the SSRPA equation serves as a good approximation for describing the responses to two-body external fields. However, this approximation offers little computational benefit, since the dimension of the $2p-2h$ space is much larger than

that of the $1p-1h$ space.

2. SSRPA calculation

Figure 5 shows the strength distributions of the two-body external fields defined in Eqs. (13)–(15) in ^{16}O , calculated by SSRPA. Figure 5(a) presents the strength distribution of the $J^\pi = 0^+$ component of the double IS 0^+ excitations given in Eq. (13). The strength distribution obtained with SSRPA_F differs significantly from that of SSRPA_D. Since the primary distinction between these two calculations is the presence of the residual interaction among $2p-2h$ configurations, this comparison demonstrates that the couplings among different $2p-2h$ states plays a crucial role. As a consequence, the main strength of the double IS 0^+ excitation is shifted considerably toward lower energies relative to SSRPA_D, in a manner analogous to the coherent $1p-1h$ excitations of IS 0^+ mode. Similarly, in Fig. 5(b), the SSRPA_F strength distribution of the double IV mode is shifted to higher excitation energies than the SSRPA_D result, analogous to the behavior observed for the IV dipole mode. A qualitatively similar trends is also found for the double IS 2^+ excitations shown in Fig. 5(c).

As shown in Figs. 1–3, that coupling among the $2p-2h$ configurations also affects the strength distributions induced by one-body external fields. Its impact on responses to two-body external fields is, however, even more pronounced, and the underlying physics appears to be more intricate. For instance, Fig. 5(a) shows main peaks around 25 MeV together with substantial strength above 80 MeV, well beyond the main peak region of SSRPA_D, which appears around $\hbar\omega = 50$ MeV. In contrast, in Fig. 5(b) the SSRPA_F strength distribution is shifted to higher excitation energies relative to SSRPA_D, indicating that the dominant contribution of the residual interaction acts repulsively. To further quantify this behavior, we examined the matrix elements of the residual interaction. Although we do not present these distributions explicitly in figures or tables, we note that they are centered near zero but exhibit a slight negative bias for interactions among nn and pp configurations and a slight positive bias for those among np configurations. Although a complete analysis is difficult due to the enormous configuration space and the complicated couplings involved, these trends are consistent with the behavior observed in Fig. 5 and help us to gain a qualitative understanding of the observed resonance shifts.

Table III summarizes the center energies and widths extracted from the Lorentzian fits ($E_c^{(2)}$ and $\Gamma^{(2)}$), and centroid energies (m_1/m_0) of the 0^+ component of the double-multipole modes obtained from SSRPA_F. Because the double IS 0^+ and 2^+ distributions in Fig. 5 can be separated into two groups (a low-energy group around $\hbar\omega \sim 30$ MeV and a broader high-energy component), we list the corresponding quantities for the first and second groups separately. We find that the center energies of

TABLE III. Center energies $E_c^{(2)}$ and widths $\Gamma^{(2)}$ extracted from the Lorentzian fits, and centroid energy m_1/m_0 of the 0^+ component of the corresponding double multipole modes obtained from SSRPA_F. Because the strength distributions for the double IS 0^+ and 2^+ in Fig. 5 can be separated into two groups, we list the corresponding quantities for the first and second groups. All values are given in MeV.

Mode	SSRPA _F				m_1/m_0
	$E_c^{(2)}$	first group	$E_c^{(2)}$	second group	
double IS 0^+	25.3	3.7	57.7	44.1	45.4
double IV 1^-	42.5	12.8	-	-	44.8
double IS 2^+	33.7	2.9	55.5	30.3	50.3

the double IS 0^+ and 2^+ modes are less than twice those of the corresponding one-body excitations obtained with RPA and SSRPA_F (Table I). These observations suggest that the residual interaction among $2p-2h$ configurations induces non-negligible correlations between the two underlying $1p-1h$ excitations, thereby going beyond a simple picture of independent double-phonon excitations, at least for the ^{16}O channels considered here. In contrast, the center energy of the double IV 1^- mode is only slightly larger than twice the corresponding one-body value. When we focus on the centroid energies, the double IS 0^+ and IV 1^- results obtained with SSRPA_F are close to the corresponding RPA values, whereas the double IS 2^+ result is larger than the RPA value but remains close to SSRPA_F one.

3. Effectiveness of subtraction method

As discussed in the previous section, the $1p-1h$ excitations can be effectively decoupled from the $2p-2h$ ones and the results of strength distributions are almost the same between HF and SSRPA_D. This indicates that the subtraction method has essentially no impact on the strength distributions induced by two-body external fields, because the subtraction modifies only the residual interaction among the $1p-1h$ configurations, as shown in Eq. (5). To verify this explicitly, we performed the same calculation without the subtraction method, denoted as SRPA, and the results are shown in Fig. 5. The strength distributions obtained with SRPA and SSRPA_F are almost indistinguishable, confirming that the subtraction method does not influence the response to two-body external fields. Only a minor modification is found for the double IS 0^+ excitation around $\hbar\omega = 16$ MeV.

C. Collectivity of resonances induced by two-body external fields

The single transition amplitudes defined in Eqs. (7) and (8) provide detailed information on the structure of

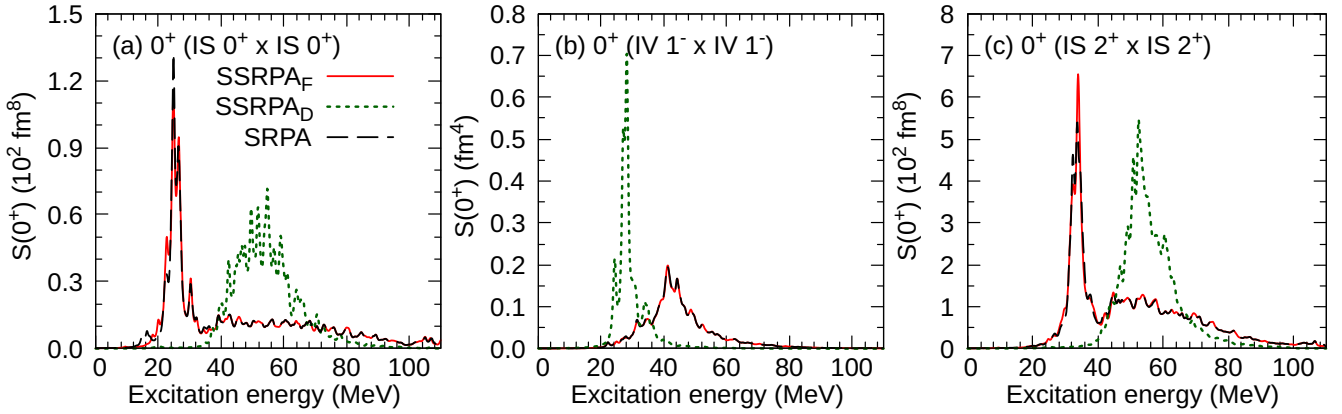


FIG. 5. Strength distributions for the two-body external fields defined in Eqs. (13)–(15) in ^{16}O . Results from SSRPA_F, SSRPA_D, and SRPA calculations are compared.

each resonance, including its degree of collectivity and the dominant particle-hole configurations that contribute to the excited state. In this section, we focus on several representative resonances induced by the two-body external fields shown in Fig. 5 and analyze their single transition amplitudes.

We first discuss the low-lying resonance at $\hbar\omega = 24.8$ MeV, which correspond to the main peak of the 0^+ component of the double IS 0^+ excitation. Figure 6 shows the single transition amplitudes C , defined in Eq. (10), as a function of the unperturbed $2p$ - $2h$ energy. As explained in the previous section, two-body excitations can be classified into three types of $2p$ - $2h$ configurations: proton-proton (pp), neutron-neutron (nn), and neutron-proton (np). The upper panel of Fig. 6 displays the nn and pp configurations, while the lower panel shows the np configurations. The solid line denotes the cumulative sum of the single transition amplitudes up to a given unperturbed $2p$ - $2h$ energy. We find that the single transition amplitude receives sizable contributions from a wide range of unperturbed energies, and that most amplitudes have the same sign, indicating that this resonance is formed constructively from many $2p$ - $2h$ configurations. This behavior is consistent with the fact that the double IS 0^+ mode involves $2\hbar\omega$ configurations and therefore can draw non-negligible strength from relatively high-lying $2p$ - $2h$ states. Furthermore, this 24.8 MeV resonance does not emerge when the calculation is performed within a reduced model space. The cumulative contributions from the $nn+pp$ configurations are comparable in magnitude to those from the np configurations: $\sum C = -4.024$ for $nn+pp$ and $\sum C = -4.155$ for np . As discussed in Sec. III B 2, the residual interaction among nn and pp configurations exhibits a slight attractive tendency (i.e., matrix elements biased toward negative values), which favors a downward shift of the resonance relative to SSRPA_D. In contrast, the np configurations tend to act repulsively and push the strength to higher excitation energies. Table IV lists representative $2p$ - $2h$ configurations contributing to the low-lying resonance of the double IS 0^+ .

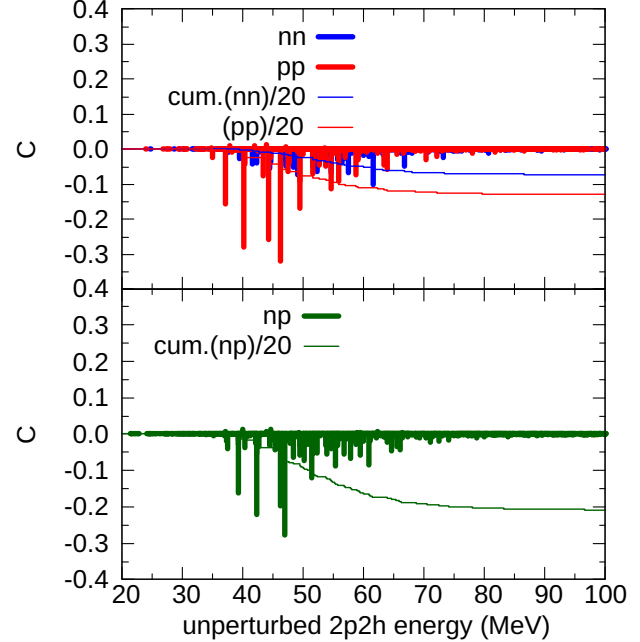


FIG. 6. Single transition amplitude $C_{\nu; p_1 p_2 h_1 h_2}$ contributing to the double IS 0^+ resonance at $\hbar\omega = 24.8$ MeV. The upper panel shows the proton-proton (pp) and neutron-neutron (nn) $2p$ - $2h$ configurations, while the lower panel displays the neutron-proton (np) $2p$ - $2h$ configurations. The solid curve represents the cumulative sum of the amplitudes, divided by 20, as a function of the unperturbed $2p$ - $2h$ energy.

rection of the energy shift correlates with the balance of the single transition amplitudes: when the cumulative contribution from $nn+pp$ configurations is comparable to that from np configurations, the strength tends to be shifted lower energies than in SSRPA_D. Conversely, when the np contribution is dominant, the strength distribution is pushed toward higher excitation energies. Table IV lists representative $2p$ - $2h$ configurations contributing to the low-lying resonance of the double IS 0^+ .

TABLE IV. Single transition amplitude of double IS 0^+ excitation at for $\hbar\omega = 24.8$ MeV.

2p-2h configuration	E_{2p2h}	$C_{\nu;p_1p_2h_1h_2}$
$([2p_{1/2}][0p_{3/2}]^{-1})_\pi ([3p_{3/2}][0p_{1/2}]^{-1})_\pi$	40.15	-0.281
$([3p_{3/2}][0p_{3/2}]^{-1})_\nu ([2p_{1/2}][0p_{1/2}]^{-1})_\pi$	42.22	-0.222
$([2p_{1/2}][0p_{3/2}]^{-1})_\pi ([4p_{3/2}][0p_{1/2}]^{-1})_\pi$	44.22	-0.258
$([4p_{3/2}][0p_{3/2}]^{-1})_\nu ([2p_{1/2}][0p_{1/2}]^{-1})_\pi$	46.24	-0.196
$([1s_{1/2}][0s_{1/2}]^{-1})_\pi ([2p_{1/2}][0p_{1/2}]^{-1})_\pi$	46.25	-0.320
$([1s_{1/2}][0s_{1/2}]^{-1})_\nu ([2p_{1/2}][0p_{1/2}]^{-1})_\pi$	46.96	-0.278

mode at $\hbar\omega = 24.8$ MeV shown in Fig. 6. In particular, the proton $[2p_{1/2}][0p_{1/2}]^{-1}$ configuration, which is one of the dominant components of the IS 0^+ strength observed in Fig. 1, play an important role in this resonance through its coupling with other $1p-1h$ configurations. Thus, this resonance can be interpreted, to a good approximation, as a double IS 0^+ excitation built on top of proton $[2p_{1/2}][0p_{1/2}]^{-1}$ configuration.

Figure 7 shows the single transition amplitudes and their cumulative sum for the higher-lying resonance at $\hbar\omega = 80.6$ MeV in the double IS 0^+ excitation. In this case, the amplitudes associated with the np configurations are dominant, while those from the nn and pp configurations are comparatively small. Consequently, the corresponding strength is shifted to higher excitation energy than in SSRPA_D. Unlike the low-lying resonance in Fig. 6, the amplitudes contributing to this high-lying resonance are broadly distributed, with comparable contributions arising from a wide range of configurations. In other words, this resonance is not characterized by a small set of specific $1p-1h$ sub-configurations that drive the IS giant monopole resonance; rather, it is built from a more uniformly distributed superposition of many $2p-2h$ configurations. A similar pattern is found for the double IS 2^+ excitation, both for the low-lying main peak and for the higher-lying resonances. Therefore, we do not repeat the discussion here.

Figure 8 shows the single transition amplitudes and their cumulative sums of the double IV 1^- excitation at $\hbar\omega = 40.4$ MeV. Most of the individual $2p-2h$ transition amplitudes for the nn , pp , and np configurations are negative, and the resonance is formed constructively from these amplitudes. The amplitudes associated with the np configurations are clearly larger than those from the nn and pp configurations, indicating that the double IV 1^- mode is dominated by particle-hole excitations involving different nucleon species. The total transition amplitude summed over $2p-2h$ configurations is $\sum C_{\nu;p_1p_2h_1h_2} = -0.0373$ for the $nn+pp$ configurations, whereas it is $\sum C_{\nu;p_1p_2h_1h_2} = -0.0909$ for the np configurations. As discussed above, the predominantly repulsive character of the np channel shifts the strength to higher excitation energies compared with the SSRPA_D result. Table V lists representative leading configurations for this resonance. The neutron and proton $[0d_{5/2}][0p_{3/2}]^{-1}$ configurations, which are one of the dominant components

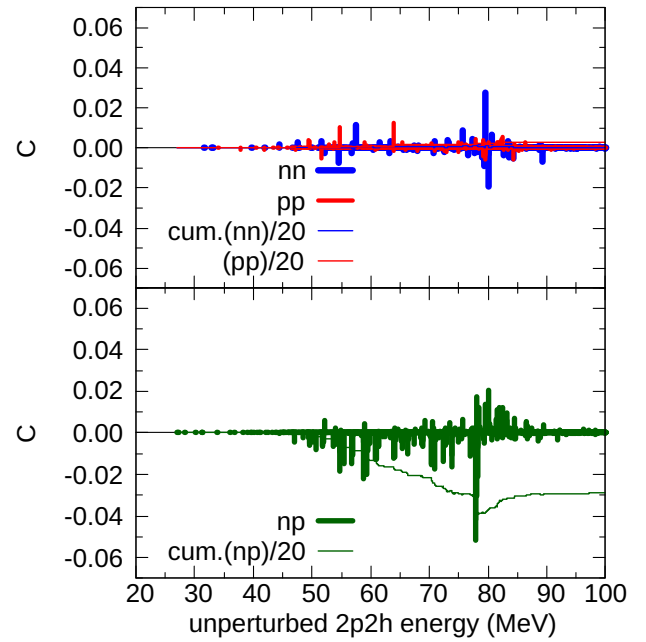


FIG. 7. Same as Fig. 6, but for the double IS 0^+ excitation at $\hbar\omega = 80.6$ MeV.

TABLE V. Single transition amplitude of double IV 1^- excitation at for $\hbar\omega = 40.4$ MeV.

2p-2h configuration	E_{2p2h}	$C_{\nu;p_1p_2h_1h_2}$
$([0d_{5/2}][0p_{3/2}]^{-1})_\nu ([0d_{5/2}][0p_{3/2}]^{-1})_\pi$	26.96	-0.0186
$([0d_{5/2}][0p_{1/2}]^{-1})_\nu ([1d_{3/2}][0p_{3/2}]^{-1})_\pi$	28.05	-0.0135
$([0d_{5/2}][0p_{3/2}]^{-1})_\pi ([1d_{3/2}][0p_{1/2}]^{-1})_\pi$	27.92	-0.0117
$([0d_{5/2}][0p_{3/2}]^{-1})_\nu ([0d_{3/2}][0p_{1/2}]^{-1})_\nu$	28.48	-0.0220
$([0d_{3/2}][0p_{3/2}]^{-1})_\nu ([0d_{5/2}][0p_{1/2}]^{-1})_\pi$	28.35	-0.0205

of the IV 1^- strength observed in Fig. 2, play an important role in this resonance through their coherent coupling with other $1p-1h$ configurations. Thus, similar to the mechanism found in the double IS 0^+ excitation, this resonance may be interpreted as a double IV 1^- excitation built on top of these underlying single IV dipole configurations.

The enhanced contribution of the np configurations to the high-lying resonances can be qualitatively understood from the behavior of the corresponding state densities. Fig. 9 shows the state densities of the $^{16}\text{O}(0^+)$ $2p-2h$ configurations for the nn , pp , and np sectors as a function of unperturbed $2p-2h$ energy, using an energy bin of 2 MeV. Up to about 40 MeV, the combined state density of the nn and pp configurations is comparable to that of the np configurations. Above 40 MeV, however, the state density of the np configurations becomes larger by a factor of 2-3 compared with the sum of the $nn+pp$ contributions. This behavior arises naturally from the Pauli exclusion principle. Once a nucleon is excited to from $1p-1h$ configuration, the occupied and unoccupied states for a second identical nucleon (nn or pp) are restricted, re-

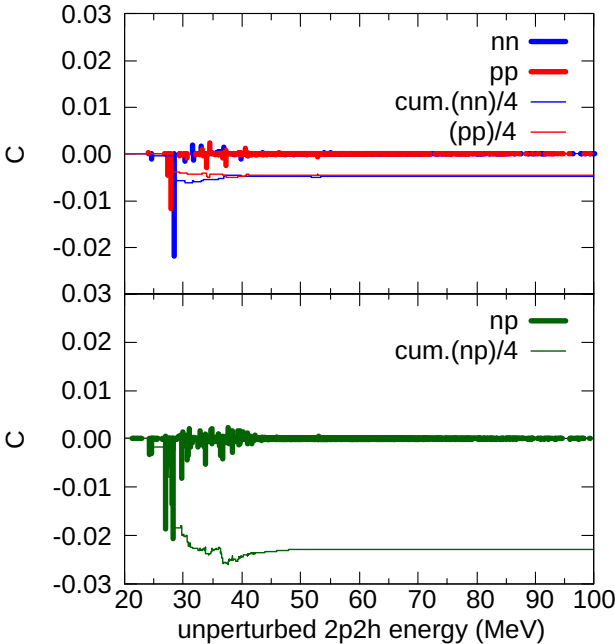


FIG. 8. $2p-2h$ configurations contributing the resonance of double IV 1^- excitation at $\hbar\omega = 40.4$ MeV. The solid line shows the cumulative sum divided by 4 up to a given unperturbed $2p-2h$ energy.

ducing the number of available $2p-2h$ configurations. In contrast, such blocking does not occur between neutrons and protons, so the number of possible np configurations remains much larger, especially at higher excitation energies. As a consequence, high-lying resonances are predominantly built from neutron-proton $2p-2h$ configurations. We note that in the present calculation the continuum single-particle spectrum is discretized by using a finite box, and the resulting state density is constructed from these discretized levels. Nevertheless, the relative behavior, namely the significantly larger np state density compared with nn and pp at high energies, is expected to remain qualitatively unchanged even under an exact treatment of the continuum.

IV. SUMMARY

We investigate nuclear responses to two-body external fields, interpreted as double-phonon excitations, in ^{16}O within the subtracted second random-phase approximation (SSRPA). To clarify the baseline behavior, we first compare Hartree-Fock results with those obtained using SSRPA with the diagonal-approximation. Their strength distributions nearly coincide for the two-body fields, indicating that residual interactions in the $1p-1h$ sector, as well as the subtraction procedure (which modifies only that sector), have only a limited influence in this channel. This behavior contrasts with one-body excitations, where the coupling between $1p-1h$ and $2p-2h$ configura-

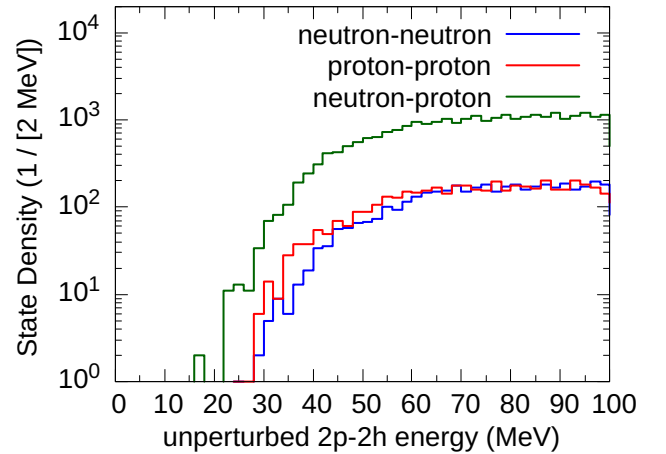


FIG. 9. 0^+ state densities of neutron-neutron (nn), proton-proton (pp), and neutron-proton $2p-2h$ configurations as a function of unperturbed $2p-2h$ energy. Energy bin is set to be 2 MeV.

tions is essential for generating collectivity and damping patterns.

When the full SSRPA calculation is performed, including couplings among different $2p-2h$ configurations through the residual interaction in $A_{22'}$, the two-body strength distributions are significantly reshaped. The double IS 0^+ and 2^+ modes show strong redistribution: their main peaks are shifted to lower energies and substantial additional strength emerges at high excitation energies, suggesting the coexistence of attractive and repulsive components in the residual interaction. In contrast, the double IV 1^- mode is pushed to higher energies, consistent with a predominantly repulsive contribution, particularly in channels dominated by neutron-proton configurations.

An analysis of single transition amplitudes reveals that low-lying resonances are built constructively from many $2p-2h$ configurations spread over a wide unperturbed energy range, with comparable cumulative contributions from nn/pp and np components, whereas high-lying resonances are dominated by np configurations owing to their larger state density. Overall, these results demonstrate that double-phonon responses are not captured by a simple folding of one-body strength functions, and that explicit $2p-2h$ mixing treated in SSRPA is indispensable for a microscopic description.

In this work, we focused on ^{16}O and restricted our analysis to the 0^+ components of the excited states. To obtain a more general perspective, it will be important to extend the study to heavier nuclei and other J^π multipoles. Nevertheless, we expect that the present findings provide a useful basis for future investigations of additional nuclei and excited states. As a next step, We plan to explore microscopic MEC effects in muon-capture reactions within the same theoretical framework.

ACKNOWLEDGMENTS

The author thanks H. Sagawa and C. L. Bai for their technical support with the SSRPA formalism. This work was supported by JSPS KAKENHI Grant Numbers JP23K03426, JP24K00647, and 25H00641, and by JST ERATO Grant No. JPMJER2304, Japan.

[1] D. Bohm and D. Pines, A collective description of electron interactions: Iii. coulomb interactions in a degenerate electron gas, *Phys. Rev.* **92**, 609 (1953).

[2] A. Bohr and B. Mottelson, *Nuclear Structure Volume II: Nuclear Deformations* (Benjamin, New York, 1975).

[3] P. Ring and P. Schuck, *The Nuclear Many-Body Problem* (Springer-Verlag, Berlin, 1980).

[4] G. Bertsch and S. Tsai, A study of the nuclear response function, *Physics Reports* **18**, 125 (1975).

[5] M. Ichimura, H. Sakai, and T. Wakasa, Spin-isospin responses via (p, n) and (n, p) reactions, *Progress in Particle and Nuclear Physics* **56**, 446 (2006).

[6] M. Matsuo, Continuum quasiparticle random-phase approximation for astrophysical direct neutron capture reactions on neutron-rich nuclei, *Phys. Rev. C* **91**, 034604 (2015).

[7] T. Saito and M. Matsuo, Continuum random-phase approximation for (n, γ) reactions on neutron-rich nuclei: Collective effects and resonances, *Phys. Rev. C* **107**, 064607 (2023).

[8] M. Dupuis, Microscopic description of elastic and direct inelastic nucleon scattering off spherical nuclei, *Eur. Phys. J. A* **53**, 1 (2017).

[9] M. Dupuis, R. Capote, T. Kawano, M. Kerveno, P. Dessagne, G. Henning, and S. Hilaire, Microscopic modeling of direct pre-equilibrium emission: Impact on exclusive and inclusive (n, xn) and fission channels, *EPJ Web Conf.* **292**, 04003 (2024).

[10] J. Da Providênci, Variational approach to the many-body problem, *Nuclear Physics* **61**, 87 (1965).

[11] J. Wambach, Damping of small-amplitude nuclear collective motion, *Reports on Progress in Physics* **51**, 989 (1988).

[12] S. Drożdż, S. Nishizaki, J. Speth, and J. Wambach, The nuclear response within extended rpa theories, *Physics Reports* **197**, 1 (1990).

[13] S. Ait-Tahar and D. Brink, Second rpa calculations of the charge-exchange quadrupole response functions in closed-shell nuclei, *Nuclear Physics A* **560**, 765 (1993).

[14] D. Gambacurta, M. Grasso, and F. Catara, Residual interaction in second random-phase approximation with density-dependent forces: rearrangement terms, *Journal of Physics G: Nuclear and Particle Physics* **38**, 035103 (2011).

[15] P. Papakonstantinou and R. Roth, Second random phase approximation and renormalized realistic interactions, *Physics Letters B* **671**, 356 (2009).

[16] P. Papakonstantinou and R. Roth, Large-scale second random-phase approximation calculations with finite-range interactions, *Phys. Rev. C* **81**, 024317 (2010).

[17] V. I. Tselyaev, Quasiparticle time blocking approximation within the framework of generalized green function formalism, *Phys. Rev. C* **75**, 024306 (2007).

[18] D. Gambacurta, M. Grasso, and J. Engel, Subtraction method in the second random-phase approximation: First applications with a skyrme energy functional, *Phys. Rev. C* **92**, 034303 (2015).

[19] M. J. Yang, C. L. Bai, H. Sagawa, and H. Q. Zhang, Effects of the skyrme tensor force on 0^+ , 2^+ , and 3^- states in ^{16}O and ^{40}Ca nuclei within the second random-phase approximation, *Phys. Rev. C* **103**, 054308 (2021).

[20] D. Gambacurta, M. Grasso, and O. Vasseur, Electric dipole strength and dipole polarizability in ^{48}Ca within a fully self-consistent second random phase approximation, *Physics Letters B* **777**, 163 (2018).

[21] D. Gambacurta, M. Grasso, and J. Engel, Gamow-Teller Strength in ^{48}Ca and ^{78}Ni with the Charge-Exchange Subtracted Second Random-Phase Approximation, *Phys. Rev. Lett.* **125**, 212501 (2020).

[22] M. J. Yang, C. L. Bai, H. Sagawa, and H. Q. Zhang, Gamow-teller transitions in magic nuclei calculated by the charge-exchange subtracted second random-phase approximation, *Phys. Rev. C* **106**, 014319 (2022).

[23] D. Gambacurta and M. Grasso, Quenching of Gamow-Teller strengths and two-particle–two-hole configurations, *Phys. Rev. C* **105**, 014321 (2022).

[24] M. J. Yang, H. Sagawa, C. L. Bai, and H. Q. Zhang, Effects of two-particle–two-hole configurations and tensor force on β decay of magic nuclei, *Phys. Rev. C* **107**, 014325 (2023).

[25] G. Colò, H. Sagawa, and P. F. Bortignon, Effect of particle-vibration coupling on single-particle states: A consistent study within the skyrme framework, *Phys. Rev. C* **82**, 064307 (2010).

[26] Y. F. Niu, G. Colò, M. Brenna, P. F. Bortignon, and J. Meng, Gamow-teller response within skyrme random-phase approximation plus particle-vibration coupling, *Phys. Rev. C* **85**, 034314 (2012).

[27] E. Litvinova, P. Ring, and V. Tselyaev, Relativistic quasiparticle time blocking approximation: Dipole response of open-shell nuclei, *Phys. Rev. C* **78**, 014312 (2008).

[28] F. Catara, P. Chomaz, and N. Van Giai, Electromagnetic decay of two-phonon states, *Physics Letters B* **277**, 1 (1992).

[29] V. V. Severyukhin, A. P. ad Voronov and N. Van Giai, Effects of phonon-phonon coupling on low-lying states in neutron-rich sn isotopes, *The European Physical Journal A - Hadrons and Nuclei* **22**, 397 (2004).

[30] E. Litvinova, P. Ring, and V. Tselyaev, Relativistic two-phonon model for the low-energy nuclear response, *Phys. Rev. C* **88**, 044320 (2013).

[31] D. Gambacurta, F. Catara, M. Grasso, M. Sambataro, M. V. Andrés, and E. G. Lanza, Nuclear excitations

as coupled one and two random-phase-approximation modes, *Phys. Rev. C* **93**, 024309 (2016).

[32] N. N. Arsenyev and A. P. Severyukhin, Isoscalar giant monopole resonance in $^{40,48}\text{Ca}$, *Journal of Physics: Conference Series* **2586**, 012047 (2023).

[33] M. Tohyama, Collectivity of double giant resonances in extended rpa theories, *Phys. Rev. C* **64**, 067304 (2001).

[34] H. Emling, Electromagnetic excitation of the two-phonon giant dipole resonance, *Progress in Particle and Nuclear Physics* **33**, 729 (1994).

[35] P. Chomaz and N. Frascaria, Multiple phonon excitation in nuclei: experimental results and theoretical descriptions, *Physics Reports* **252**, 275 (1995).

[36] D. H. Dowell, G. Feldman, K. A. Snover, A. M. Sandorfi, and M. T. Collins, Excited-state giant dipole resonances in (p, γ) : A new probe of single-particle strengths, *Phys. Rev. Lett.* **50**, 1191 (1983).

[37] C. A. Bertulani and G. Baur, Electromagnetic processes in relativistic heavy ion collisions, *Physics Reports* **163**, 299 (1988).

[38] C. Bertulani and V. Ponomarev, Microscopic studies on two-phonon giant resonances, *Physics Reports* **321**, 139 (1999).

[39] H. Esbensen, Sensitivity to multi-phonon excitations in heavy-ion fusion reactions, *Phys. Rev. C* **72**, 054607 (2005).

[40] N. Auerbach, Isotensor double giant resonances in double charge-exchange reactions, *Annals of Physics* **197**, 376 (1990).

[41] K. Muto, Sum rules for double gamow - teller excitation, *Physics Letters B* **277**, 13 (1992).

[42] F. Andreozzi, F. Knapp, N. L. Iudice, A. Porrino, and J. Kvasil, Exact formulation and solution of the nuclear eigenvalue problem in a microscopic multiphonon space, *Phys. Rev. C* **75**, 044312 (2007).

[43] V. Ponomarev and V. Voronov, On double resonances in spherical nuclei, *Physics Letters B* **279**, 1 (1992).

[44] C. Bertulani and V. Zelevinsky, Excitation of multiphonon giant resonance states in relativistic heavy-ion collisions, *Nuclear Physics A* **568**, 931 (1994).

[45] V. Y. Ponomarev, E. Vigezzi, P. F. Bortignon, R. A. Broglia, G. Colò, G. Lazzari, V. V. Voronov, and G. Baur, Multiple excitation of giant dipole resonances in relativistic heavy ion collisions, *Phys. Rev. Lett.* **72**, 1168 (1994).

[46] F. Minato, T. Naito, and O. Iwamoto, Nuclear many-body effects on particle emission following muon capture on ^{28}Si and ^{40}Ca , *Phys. Rev. C* **107**, 054314 (2023).

[47] M. Lifshitz and P. Singer, Nuclear excitation function and particle emission from complex nuclei following muon capture, *Phys. Rev. C* **22**, 2135 (1980).

[48] C. Yannouleas, Zero-temperature second random phase approximation and its formal properties, *Phys. Rev. C* **35**, 1159 (1987).

[49] N. Van Giai and H. Sagawa, Spin-isospin and pairing properties of modified skyrme interactions, *Physics Letters B* **106**, 379 (1981).

[50] D. Gambacurta, M. Grasso, and F. Catara, Collective nuclear excitations with skyrme-second random-phase approximation, *Phys. Rev. C* **81**, 054312 (2010).

[51] G. Scamps and D. Lacroix, Systematics of isovector and isoscalar giant quadrupole resonances in normal and superfluid spherical nuclei, *Phys. Rev. C* **88**, 044310 (2013).